Fatigue Crack Propagation of Multiple Coplanar Cracks with the Coupled Extended Finite Element/Fast Marching Method

D. L. Chopp [a,*,1] and N. Sukumar [b]

[a] *Engineering Sciences and Applied Mathematics Dept., Northwestern University, Evanston, IL 60208-3125*

[b] *Department of Civil and Environmental Engineering, University of California, Davis, CA 95616*

Abstract

A numerical technique for modeling fatigue crack propagation of multiple coplanar cracks is presented. The proposed method couples the Extended Finite Element Method (X-FEM) [40] to the Fast Marching Method (FMM) [34]. The entire crack geometry, including one or more cracks, is represented by a single signed distance (level set) function. Merging of distinct cracks is handled naturally by the fast marching method with no collision detection or mesh reconstruction required. The fast marching method in conjunction with the Paris crack growth law is used to advance the crack front. In the X-FEM, a discontinuous function and the two-dimensional asymptotic crack-tip displacement fields are added to the finite element approximation to account for the crack using the notion of partition of unity [20]. This enables the domain to be modeled by a single fixed finite element mesh with no explicit meshing of the crack surfaces. In an earlier study [39], the methodology, algorithm, and implementation for three-dimensional crack propagation of single cracks was introduced. In this paper, simulations for multiple planar cracks are presented, with crack merging and fatigue growth carried out without any user-intervention or remeshing.

Key words: partition of unity, extended finite element method, fast marching method, level set method, fatigue crack growth, coplanar cracks in 3-d

* Corresponding author.
Email address: chopp@northwestern.edu (D. L. Chopp).

[1] This work was supported in part by the NSF/DARPA VIP program under awards DMS-9615877 and NSF DMS-9872036

1 Introduction

Numerical methods for capturing moving interfaces have played a vital role in a broad range of modeling applications from multi-phase fluid flow to thin-film deposition and etching. In many of these applications, solution of an elliptic equation involving irregularly shaped moving boundaries is required in order to obtain the velocity field of the interface. Many different techniques are available, each with their own strengths and weaknesses making no single technique optimal for all moving interface problems.

In this paper, we present a recently developed numerical method, which has a different set of strengths than existing methods. It is the result of coupling a popular interface capturing method, the fast marching method (FMM) [32,33,8], with an extended form of the classical finite element method, the Extended Finite Element Method (X-FEM) [22,40]. The two methods form a natural partnership for capturing a monotonically advancing front which requires a coupled elliptic equation solution for determining the front velocity. In the FMM, the motion of the interface is embedded in the solution φ of a static Hamilton-Jacobi equation which describes the position of the interface at time t by the level contour $\varphi(\mathbf{x}) = t$. This function φ is computed using a single pass through the mesh by carefully selecting the order in which the nodal values are evaluated. In the X-FEM, additional non-linear functions are added to the finite element approximation to account for the interface using the notion of partition of unity. This enables the domain to be modeled by finite elements with no explicit meshing of the crack surfaces. In the coupled method, the FMM maintains the location and motion of the crack front whereas the X-FEM is used to compute the local front velocity. For a treatment of non-monotonically advancing fronts, the fast marching method is replaced by the level set method [28], see [19].

In [39], Sukumar and co-workers applied this algorithm to single planar three-dimensional fatigue cracks. In that paper, the accuracy of the SIF calculations, as well as the algorithm as a whole, tested favorably against the known solution of a single circular penny crack embedded in an infinite domain. A sample of the results are shown in Fig. 1. However, that algorithm was not able to handle multiple cracks which may merge as they grow. The ease with which the fast marching method can handle merging interfaces is one of its strongest features, but difficulties remain in the corresponding implementation of the X-FEM. At issue is how to properly employ the X-FEM when separate interfaces, such as distinct cracks, approach each other.

In this paper, we give an overview of the original method, then describe how to incorporate multiple cracks which are able to coalesce. We begin by describing existing numerical methods for modeling fatigue cracks and then give

a description of both the X-FEM in Section 3 and the FMM in Section 4. In Section 5.1, the enrichment functions that appear in the displacement-based finite element approximations are discussed. The fast marching method in conjunction with the Paris crack growth law is used to advance the crack front (Section 5.4). The governing equations of elastostatics and the associated weak form are presented in Section 6. In Section 7, fatigue crack growth simulations for multiple planar cracks are presented, with crack merging and fatigue growth carried out without any user-intervention or remeshing.

2 Review of Numerical Methods for Fatigue Crack Propagation

Failure in engineering structures is very often caused by defects such as cracks that grow beyond a safety-critical size. Initial defects such as pre-cracks are present in structures as fabrication defects during manufacturing, or due to localized damage during service. Fatigue crack growth is one of the principle modes of failure for structures under cyclic loading conditions. Damage tolerant assessment of structures provides a means to assess the critical crack size that is tolerable from the viewpoint of structural strength, and also the number of cycles to eventual failure. Numerical simulations using the principles of linear elastic fracture mechanics provide a sound tool to carry out damage tolerant analyses, and hence the development of numerical models for three-dimensional crack growth of multiple cracks and their interactions is important.

Exact solutions for the evolution of arbitrary-shaped cracks in 3-dimensional structural components are not available, and hence numerical methods are the only recourse for three-dimensional fatigue crack growth simulations. Some of the prominent numerical methods used for modeling fatigue crack growth are: finite element and boundary element methods [15,21,6,11,7], boundary integral equations [42], finite element alternating method [41,26], and the dislocation distribution approach [18,9]. Much of the progress in finite element remeshing algorithms and the capability to carry out three-dimensional crack modeling and fatigue crack propagation in complex structural components is due to contributions of the Cornell Fracture Group [2]. The finite element framework is particularly attractive for it provides the ease and flexibility of modeling complex structural components with arbitrary boundary conditions, nonlinear material behavior, and anisotropic material properties. In spite of the successes achieved in computational fracture mechanics with finite elements, mesh generation in 3-dimensions for crack growth simulations is still a formidable task. This is because in order to capture the evolution of the crack in fatigue growth simulations, remeshing along with local refinements around

[2] see `http://www.cfg.cornell.edu`

the crack front are required to obtain accurate solutions for fracture parameters such as the stress intensity factor (SIF). Hence, a computational method that can automate three-dimensional crack propagation simulations on relatively coarse meshes without the need for remeshing or user-intervention is of significance. The use of the FMM with the X-FEM removes the need to represent and maintain the geometry of the crack at every step, which is a burden in most existing numerical methods for fracture modeling.

The first three-dimensional crack modeling study using the X-FEM [40] discussed the computational geometric issues for the representation of the crack surface and its interaction with the finite element mesh for the enrichment. In [39], the methodology for crack propagation of single cracks was presented. That basic algorithm coupled with the work in [35] has led to 3-dimensional non-planar crack growth in [17]. This advance points to the promise and potential of the X-FEM towards the automated modeling of arbitrary crack propagation in 3-dimensional structural components.

3 Extended Finite Element Method

The Extended Finite Element Method (X-FEM) [22,10,40] is a numerical method to model internal (or external) boundaries such as holes, inclusions, or cracks, without requiring the mesh to conform to these boundaries. The X-FEM is based on a standard Galerkin procedure, and uses the concept of partition of unity [20] to accommodate the internal boundaries in the discrete model. The partition of unity method [20] generalized finite element approximations by presenting a means to embed local solutions of boundary-value problems into the finite element approximation. This idea was exploited by Oden and co-workers [27,12] for problems with internal boundaries—the numerical technique was referred to as the Generalized Finite Element Method (GFEM). Stroubolis and co-workers [36,37] have used the partition of unity framework to model holes and cracks in 2-dimensions, whereas Duarte and co-workers [13] have studied the simulation of three-dimensional dynamic crack propagation.

Partition of unity enrichment for discontinuities and near-tip crack fields was introduced in [5]. The displacement enrichment functions for crack problems are functions that span the asymptotic near-tip displacement field—see [14] for their use in the Element-Free Galerkin method. A significant improvement in discrete 2-dimensional crack growth modeling without the need for any remeshing strategy was conceived by Moës and co-workers [22], with further developments in [10] for holes and branched cracks. The generalized Heaviside step function was proposed as a means to model the crack away from the crack-tip, with simple rules for the introduction of the discontinuous and crack-tip

enrichments. The extension of the X-FEM to 3-dimensional crack problems was presented in [40]. This advance clearly provided a robust and accurate computational tool for modeling discontinuities independent of the mesh geometry. The X-FEM has been successfully applied to quasi-static and fatigue crack propagation in 2-dimensions [22,10] and 3-dimensions [40,39,23,17]. The coupling of level sets with the X-FEM for the description and evolution of cracks has also been explored in 2-dimensions [35].

The enrichment of the finite element approximation is described as follows. Consider a point $\mathbf{x}$ of $\mathbb{R}^d$ ($d = 1, 2, 3$) that lies inside a finite element e. Denote the nodal set $\mathbf{N} = \{n_1, n_2, \ldots, n_m\}$, where m is the number of nodes of element e. ($m = 2$ for a linear one-dimensional finite element, $m = 3$ for a constant-strain triangle, $m = 8$ for a trilinear hexahedral element, etc.) The enriched displacement approximation for a vector-valued function $\mathbf{u}(\mathbf{x}) : \mathbb{R}^d \to \mathbb{R}^d$ assumes the form:

$$\mathbf{u}^h(\mathbf{x}) = \underbrace{\sum_{\substack{I \\ n_I \in \mathbf{N}}} \phi_I(\mathbf{x})\mathbf{u}_I}_{classical} + \underbrace{\sum_{\substack{J \\ n_J \in \mathbf{N}^g}} \phi_J(\mathbf{x})\psi(\mathbf{x})\mathbf{a}_J}_{enriched}, \quad (\mathbf{u}_I, \mathbf{a}_J \in \mathbb{R}^d) \tag{1}$$

where the nodal set $\mathbf{N}^g$ is defined as:

$$\mathbf{N}^g = \{n_J : n_J \in \mathbf{N},\ \omega_J \cap \Omega_g \neq \emptyset\}. \tag{2}$$

In the above equation, $\omega_J = \text{supp}(n_J)$ is the support of the nodal shape function $\phi_J(\mathbf{x})$, which consists of the union of all elements with n_J as one of its vertices, or in other words the union of elements in which $\phi_J(\mathbf{x})$ is non-zero. In addition, Ω_g is the domain associated with a geometric entity such as crack-tip [22], crack surface in 3-dimensions [40], or material interface [38]. In general, the choice of the enrichment function $\psi(\mathbf{x})$ that appears in Eq. (1) depends on the geometric entity.

4 Fast Marching Method

The Fast Marching Method was first introduced by Sethian [32], and later improved by Sethian [33] and Chopp [8]. The method computes the crossing time map for a monotonically advancing front in an arbitrary number of spatial dimensions. The crossing time map is constructed by solving an equation of the form

$$\|\boldsymbol{\nabla}\varphi(\mathbf{x})\| = \frac{1}{F(\mathbf{x})}, \tag{3}$$

where $F(\mathbf{x})$ is the front speed at the point $\mathbf{x}$ and $\varphi(\mathbf{x})$ is the time at which the evolving front passes through the point $\mathbf{x}$. The initial front is then given by $\varphi^{-1}(0)$, and the level contour $\varphi^{-1}(t)$ is the location of the front at time t.

The solution of Eq. (3) is constructed by first replacing the gradient by suitable upwind operators, and then systematically advancing the front by marching outwards from the boundary data in an upwind fashion. For N nodes, the method has a total operation count of $O(N \log N)$. If $F(\mathbf{x}) \equiv 1$, then Eq. (3) becomes the Eikonal equation and the solution $\varphi(\mathbf{x})$ of Eq. (3) gives the distance from $\mathbf{x}$ to the zero contour $\varphi^{-1}(0)$. In this paper, we use this application to compute the distance map from the grid nodes to the crack front.

In the FMM, all the nodes in the mesh are sorted into three disjoint sets, the set of all *accepted nodes* A, the set of all *tentative nodes* T, and the set of all *distant nodes* D. The method systematically moves nodes from the set D to the set T and finally into the set A and terminates when all nodes are in the set A. Briefly, the set A consists of all nodes $\mathbf{x}$ whose value of $\varphi(\mathbf{x})$ has been computed, the set T consists of all nodes that are candidates for inclusion into the set A, and the set D consists of all nodes which are too far from the set A to be candidates. With these sets in mind and denoting $\mathbf{x}_{i,j}$ as the coordinate of node (i,j) and $\varphi_{i,j} \equiv \varphi(\mathbf{x}_{i,j})$, the algorithm proceeds as follows:

(1) Initialize a core set of nodes to be in the set A. The value of $\varphi(\mathbf{x})$ for $\mathbf{x} \in A$ is determined by direct computation. Each element of the mesh through which the zero contour of φ crosses, i.e. the initial front position, has each of its nodes start in the set A and the value of each node is determined by directly computing the distance from each node to the level contour in the element. We use bicubic interpolation on the rectilinear FMM grid to approximate the contour. A variant of Newton's method is used to compute the distance to that contour. For additional details, see Chopp [8].

(2) For each node $\mathbf{x} \in A$, each neighboring node $\mathbf{y} \notin A$ connected to $\mathbf{x}$ is assigned a tentative value $\varphi(\mathbf{y})$ and placed in the set T. The tentative value is constructed by using second-order one-sided finite difference approximations for Eq. (3). For example, if we wish to compute $\varphi_{i,j}$ with $\mathbf{x}_{i-1,j}$, $\mathbf{x}_{i,j+1} \in A$, then $\varphi_{i,j}$ is constructed by solving

$$\begin{aligned}&\left[\max\left(D_x^-\varphi_{i,j} + \frac{s_1^-\Delta x}{2} D_x^- D_x^- \varphi_{i,j}, -D_x^+\varphi_{i,j} + \frac{s_1^+\Delta x}{2} D_x^+ D_x^+ \varphi_{i,j}, 0\right)\right]^2 + \\ &\left[\max\left(D_y^-\varphi_{i,j} + \frac{s_2^-\Delta y}{2} D_y^- D_y^- \varphi_{i,j}, -D_y^+\varphi_{i,j} + \frac{s_2^+\Delta y}{2} D_y^+ D_y^+ \varphi_{i,j}, 0\right)\right]^2 \\ &= 1/F_{i,j}^2. \end{aligned} \tag{4}$$

where

$$D_x^-\varphi_{i,j} = \frac{\varphi_{i,j} - \varphi_{i-1,j}}{\Delta x}, \qquad D_x^+\varphi_{i,j} = \frac{\varphi_{i+1,j} - \varphi_{i,j}}{\Delta x}, \tag{5}$$

and

$$s_1^- = \begin{cases} 1 & \mathbf{x}_{i-1,j} \in A \\ 0 & \mathbf{x}_{i-1,j} \notin A \end{cases}, \qquad s_1^+ = \begin{cases} 1 & \mathbf{x}_{i+1,j} \in A \\ 0 & \mathbf{x}_{i+1,j} \notin A \end{cases}. \tag{6}$$

Expressions for D_y^-, D_y^+, s_2^-, s_2^+ are similar (see [33]). Equation (4) is actually a quadratic in the unknown quantity $\varphi_{i,j}$ and can be solved to produce two possible values. The larger of the two solutions is taken for $\varphi_{i,j}$. The set T is maintained as a sorted list by a heap sort method with the smallest value always at the top.

Pictorially, the set A now consists of all nodes immediately adjacent to the zero contour $\varphi^{-1}(0)$, the set T is a thin layer of nodes surrounding the nodes in A, and the set D is everything else (Fig. 2).

(3) The main loop now begins by taking the node $\mathbf{x} \in T$ with the smallest value for $\varphi(\mathbf{x})$ and moves it from the set T to the set A.

(4) Each node $\mathbf{y}$ adjacent to the node $\mathbf{x}$ selected in step 3, and not already in A, has its value $\varphi(\mathbf{y})$ updated using Eq. (4). If $\mathbf{y} \in T$, then T must be re-sorted to account for the changed value of $\varphi(\mathbf{y})$. If $\mathbf{y} \in D$, it is moved from D to T.

(5) If $T \neq \emptyset$, then go to step 3

For further information regarding the fast marching method and the level set method, see [34].

5 Three-Dimensional Crack Modeling

The merits of coupling level sets to the extended finite element method was first explored in [38] to model static material interfaces, and subsequently its advantages further realized in [39,35,23,17] for modeling crack discontinuities. The advantages that accrue by using the level set framework in the X-FEM are the following:

(1) Level sets provide greater ease and simplification in the representation of geometric entities such as holes, inclusions (material interfaces) and cracks, which are typically encountered in solid mechanics applications. Instead of a simplex or Bézier surface representation of the geometry, now a simple function-representation (level set φ) is used, which requires only the storage of signed distance values at discrete points (nodes) with finite element interpolation used to obtain the value of the level set at any point in the domain.

(2) Geometric computations for the crack in relation to the finite element mesh as well as geometric properties of the crack front (such as normal and tangent vectors) are readily computed knowing the level set function [39].

(3) The selection of nodes to be enriched and the computation of the enrichment functions for crack problems [39,35] or material interfaces [38,19] use the level set function(s).

(4) For crack modeling in 3-dimensions, the level sets also provide a means to

easily compute the local orthogonal crack front coordinate system that is required for stress intensity factor computations using domain integral representations [39,23,17]. This task is presently carried out using Newton's method (iterative procedure) in 3-dimensional fracture computations using finite element techniques [16].

Geometric issues associated with the representation of the crack surface, the evolution of the crack front, and the merging of multiple cracks, are all resolved by using level set (signed distance) functions and the fast marching method. All the cracks are represented by a single two-dimensional signed distance function corresponding to the crack plane. In the X-FEM, each crack is modeled by enriching the nodes whose nodal shape function supports intersect the interior of the crack. The selection of nodes for enrichment as well as the computation of enrichment functions is carried out using signed distance functions. In addition to the above, partitioning algorithms are also implemented if the crack intersects the finite elements—see [40] for details. In the following, we restrict the description of the implementation to planar cracks (x_1-x_2 plane) in three dimensions.

5.1 Enrichment Functions

Consider a single crack in 3-dimensions, and let Γ_c be the crack surface and Λ_c the crack front. Note that for an internal crack, the crack front corresponds to the boundary of the crack: $\Lambda_c = \partial\Gamma_c$ whereas for an edge crack, the crack front is only part of the boundary: $\Lambda_c \subset \partial\Gamma_c$. The interior of a planar crack is modeled by the enrichment function $H(\mathbf{x})$, which we refer to as a generalized Heaviside step function. The function $H(\mathbf{x})$ takes on the value $+1$ above the crack and -1 below the crack. More precisely, let $\mathbf{x}^*$ be the closest point to $\mathbf{x}$ on the crack Γ_c, and $\mathbf{n}$ be the normal to the crack plane (Fig. 3). The $H(\mathbf{x})$ function is then given by

$$H(\mathbf{x}) = \begin{cases} 1 & \text{if } (\mathbf{x} - \mathbf{x}^*) \cdot \mathbf{n} \geq 0 \\ -1 & \text{otherwise} \end{cases} . \tag{7}$$

In the neighborhood of the crack front, the asymptotic fields are two-dimensional in nature, and enrichment functions which incorporate the radial and angular behavior of the asymptotic near-tip displacement field are used. The crack-front enrichment functions are:

$$\mathbf{\Phi}(\mathbf{x}) \equiv \{\psi_1, \psi_2, \psi_3, \psi_4\} = \left[\sqrt{r}\cos\frac{\theta}{2},\ \sqrt{r}\sin\frac{\theta}{2},\ \sqrt{r}\sin\theta\sin\frac{\theta}{2},\ \sqrt{r}\sin\theta\cos\frac{\theta}{2}\right], \tag{8}$$

where r and θ are polar coordinates in the $x_{\hat{1}}$-$x_{\hat{2}}$ plane (Fig. 3). Note that the second function in the above equation is discontinuous on the crack plane.

At any point $\mathbf{x}$, let $\mathbf{x}_p$ be the orthogonal projection of $\mathbf{x}$ onto the crack plane. Next, the signed distance function φ_1 represents the crack geometry, so $\varphi_1(\mathbf{x})$ is the signed distance from $\mathbf{x}_p$ to the crack front. Also define $\varphi_2(\mathbf{x})$ to be the signed height of $\mathbf{x}$ above or below the crack plane. Therefore, at a point $\mathbf{x}$, for which the crack front enrichment functions are to be computed, $x_{\hat{1}} = \varphi_1(\mathbf{x}_p)$, and $x_{\hat{2}} = \varphi_2(\mathbf{x})$ [39]. Using the above, the enrichment functions Eq. (7), Eq. (8) can be computed from

$$r = \sqrt{x_{\hat{1}}^2 + x_{\hat{2}}^2} = \sqrt{(\varphi_1(\mathbf{x}_p))^2 + (\varphi_2(\mathbf{x}))^2}, \tag{9}$$

$$\theta = \tan^{-1}(x_{\hat{2}}/x_{\hat{1}}) = \tan^{-1}(\varphi_2(\mathbf{x})/\varphi_1(\mathbf{x}_p)), \tag{10}$$

$$H(\mathbf{x}) = \text{sign}(\varphi_2(\mathbf{x})) = \begin{cases} 1 & \text{if } \varphi_2(\mathbf{x}) \geq 0 \\ -1 & \text{otherwise} \end{cases}. \tag{11}$$

The use of the crack-front enrichment functions serves two main purposes:

(1) sub-mesh resolution of the crack-front location; and
(2) better accuracy on relatively coarse finite element meshes [22,40].

5.2 Selection of Enriched Nodes

We next describe the enrichment for 3-dimensional crack modeling. The enriched finite element approximation is [40]:

$$\mathbf{u}^h(\mathbf{x}) = \sum_{\substack{I \\ n_I \in \mathbf{N}}} \phi_I(\mathbf{x})\mathbf{u}_I + \sum_{\substack{J \\ n_J \in \mathbf{N}^c}} \phi_J(\mathbf{x})H(\mathbf{x})\mathbf{a}_J + \sum_{\substack{K \\ n_K \in \mathbf{N}^f}} \phi_K(\mathbf{x}) \left(\sum_{l=1}^{4} \psi_l(\mathbf{x})\mathbf{b}_K^l \right). \tag{12}$$

The second and third terms on the right-hand side of the above equation are the discontinuity and front enrichments, respectively. The set $\mathbf{N}^f$ consists of those nodes for which the closure of the nodal shape function support intersects the crack front. The set $\mathbf{N}^c$ is the set of nodes whose nodal shape function support is intersected by the crack and which do not belong to $\mathbf{N}^f$:

$$\mathbf{N}^f = \{n_K : n_K \in \mathbf{N}, \bar{\omega}_K \cap \Lambda_c \neq \emptyset\}, \tag{13}$$

$$\mathbf{N}^c = \{n_J : n_J \in \mathbf{N}, \omega_J \cap \Gamma_c \neq \emptyset, n_J \notin \mathbf{N}^f\}. \tag{14}$$

By using the sign of the level set (signed distance) functions φ_1 and φ_2 (see Section 5.1), the nodal sets $\mathbf{N}^c$ and $\mathbf{N}^f$ are easily determined for a planar crack. The approach we use is similar in principle to that used in [38] to determine

the enriched nodes for a material interface. Let $\tilde{\mathbf{T}}^c$, $\mathbf{T}^f$, and $\mathbf{T}^c$ denote sets that contain a list of finite elements. For a given element e, let $\varphi_i^{\min}$, $\varphi_i^{\max}$ be the minimum and maximum values of φ_i on e. If $\varphi_2^{\min}\varphi_2^{\max} \leq 0$ and $\varphi_1^{\max} < 0$, then we add e to the set $\tilde{\mathbf{T}}^c$, whereas if $\varphi_2^{\min}\varphi_2^{\max} \leq 0$ and $\varphi_1^{\min}\varphi_1^{\max} \leq 0$, then we add e to the set $\mathbf{T}^f$. The enriched nodal set $\mathbf{N}^f$ consists of all nodes that are in the connectivity of the elements in the set $\mathbf{T}^f$. In addition, let V_J^+ and V_J^- ($V_J = V_J^- + V_J^+$) be the volumes of the support ω_J of node J above and below the crack, respectively. If $\tilde{\mathbf{N}}^c$ is the set of nodes that are in the connectivity of the elements in $\tilde{\mathbf{T}}^c$, then

$$\mathbf{N}^c = \{n_J : n_J \in \tilde{\mathbf{N}}^c,\, n_J \notin \mathbf{N}^f, V_J^+/V_J > \epsilon, V_J^-/V_J > \epsilon\}, \tag{15}$$

where $\epsilon = 10^{-4}$ is used in the computations. For an elliptical crack that is located along element facets (boundaries), the enriched nodes that lie on the crack plane are shown in Fig. 5. The mesh shown in Fig. 4 is used, with the semi-major axis $a = 0.1$ and the semi-minor axis $b = 0.05$; there are about eight elements that span the major axis of the crack. The nodes enriched by the Heaviside function are shown in Fig. 5a, whereas nodes enriched by the crack-front enrichment functions are shown in Fig. 5b. Note that the corresponding nodes that belong to the hexahedral elements above and below the crack are also enriched with the crack-front enrichment functions.

5.3 Enrichment for Multiple Cracks

For the case of m coplanar cracks, the signed distance function φ_1 represents the entire crack geometry (all m cracks on the given crack plane). Two points $\mathbf{x}_1$, $\mathbf{x}_2$ are defined to be in the same crack if there is a path from $\mathbf{x}_1$ along connected nodes to $\mathbf{x}_2$ such that each node on that path is also inside a crack (i.e. $\varphi_1(\mathbf{x}) < 0$ for all $\mathbf{x}$ along the path).

This test is computed quickly using a simple recursive paint-fill type algorithm. Each node is initially painted color 0. The mesh is searched for any node $\mathbf{x}$ with $\varphi_1(x) < 0$ and with color 0. It is then painted a new color c where c counts the number of distinct cracks found. All nodes within the same crack are recursively located and painted the same color. Once the whole crack is painted, the search for new cracks resumes, each new crack being painted a new value of c. In this way, both the number of cracks can be counted as well as each crack being properly separated.

The FMM can now be used to generate a separate distance function φ_1^i for each distinct crack i, which gives the distance to crack i independent from any other cracks. Figure 7 illustrates the resulting pair of distance functions for two neighboring cracks.

For a single convex crack front, the nodal enrichment is straightforward. However, when multiple crack fronts approach each other, the handling of the enrichment has additional complications. As illustrated in Figure 6, as two growing cracks approach each other, there can be nodes which are enriched due to proximity to two distinct crack fronts. If a single distance function φ_1 is used, then at a node which is enriched twice, an error in the evaluation of the distance can be introduced (in Figure 6 this is the case for the enrichment from the right crack front). This error will then appear in the construction and evaluation of the enriched function approximation Eq. (8) in that region. Splitting the distance function into multiple independent distance functions for each separate crack alleviates this problem. In Figure 6, this corresponds to extending the single distance function φ_1 into φ_1^1, φ_1^2 with the dashed lines. This then separates the coordinate systems for the two enrichments, correcting the error in the distance calculation at multiply-enriched nodes.

Of course, the multiple enrichment error from using only a single level set function for multiple cracks also arises for a single crack with a deep non-convexity such as at a cusp immediately after two cracks have merged. Qualitatively, the solutions we obtain still look reasonable, but there are no theoretical or computational results against which we can compare. Correcting this error is the subject of on-going research.

Apart from the difficulties associated with level set representations of merging cracks, the computation of the stress intensity factors (required to determine the velocities on the front) along the crack front also present a few theoretical as well as computational challenges. The computation of the mode I stress intensity factor K_I is based on a domain integral representation: a box (cuboid) around the point s which lies on the crack front (of say the first crack) is constructed and a volume integral is evaluated within the box to determine K_I (see [24,25]). Consider the case when two planar cracks are within some small distance ϵ ($\epsilon \lll h$) prior to merging, where h is the characteristic mesh spacing in the vicinity of the crack front. In this case, a constraint is imposed on the box dimension in the plane of the crack since the box can encompass only one discontinuity (first crack); a similar situation arises if the point s is on the crack front of the second crack. In the computations we assume normal velocity values to be such that merger takes place when the cracks are a finite distance apart. Theoretical as well as computational issues arise for the case of a single crack with a deep cusp which was alluded to in the previous paragraph. In addition, the case of three or more coplanar cracks merging also poses fundamental questions in the transition of enrichment from three cracks to just a single one. At present, some of these issues are still open questions and are not resolved in the current implementation. Possible remedies to overcome some of these situations include the development of alternative approaches to compute the stress intensity factors—as unknowns themselves in the displacement approximation, or possibly through alternative

techniques to compute the stress intensity factors.

5.4 Crack Growth Algorithm

Fatigue crack growth is assumed to be governed by the Paris law [29]:

$$\frac{da}{dN} = C(\Delta K)^m, \tag{16}$$

where C and m are material constants and ΔK is the stress intensity factor range. For the mode I problems considered here, we use $\Delta K = K_I$. Let n be the number of points on the crack front at which the SIF is evaluated, and Δa_{max} the maximum user-specified increment normal to the crack front. Then,

$$\frac{\Delta a_i}{\Delta a_{max}} = \left(\frac{K_I^i}{K_I^{max}} \right)^m, \tag{17}$$

which gives the normal growth increment at any point $\mathbf{x}_i \in \Lambda_c$ ($i = 1, 2, \ldots, n$). In the computations, for a user-specified n, the crack front is parameterized by arc length s such that s_t is the total length of the crack front. Then, $ds = s_t/n$ is used as the increment on the crack front to find the coordinates of the n points on the crack front. The complete crack growth algorithm now follows:

(1) Step $t = 0$ (t_{max} is user-specified). Let φ_1 be a level set function for the crack front(s) with $\varphi_1 = 0$ on the crack front(s), $\varphi_1 < 0$ in the crack interior, and $\varphi_1 > 0$ otherwise. For example, φ_1 for two ellipses on the x_1-x_2 plane could be

$$\varphi_1 = \min \left(\frac{(x_1 - c_1)^2}{a_1^2} + \frac{(x_2 - d_1)^2}{b_1^2} - 1, \frac{(x_1 - c_2)^2}{a_2^2} + \frac{(x_2 - d_2)^2}{b_2^2} - 1 \right). \tag{18}$$

(2) Label each distinct crack using the recursive paint-fill algorithm.

(3) Compute the signed distance function(s) φ_1^i using the FMM with $F = 1$ in Eq. (3) where ${\varphi_1^i}^{-1}(0)$ describes the crack front (zero level set curve) for the i^{th} crack as labelled in step 2. Note that the global signed distance function φ_1 is easily recovered via

$$\varphi_1 = \min_i \varphi_1^i. \tag{19}$$

(4) Evaluate the front speed F at n discrete points on the front(s). Assuming unit time increment in the FMM, we have $F_i = \Delta a_i$, where Δa_i are computed using Eq. (17).

(5) Given the distance map and a front speed function F defined on the crack front identified by $\varphi_1^{-1}(0)$, a speed function F_{ext} can be computed

by solving the equation

$$\boldsymbol{\nabla} F_{ext} \cdot \boldsymbol{\nabla} \varphi_1 = 0, \tag{20}$$

where $F_{ext}\Big|_{\varphi_1^{-1}(0)} = F\Big|_{\varphi_1^{-1}(0)}$ using the FMM [1]. The speed function so constructed is designed so that the speed is constant along lines normal to the crack front.

(6) Once F_{ext} is constructed, it is inserted into Eq. (3) and the FMM is again applied to compute the crossing time map for the advancing crack front, namely

$$\|\boldsymbol{\nabla}\psi\| = \frac{1}{F_{ext}}, \quad \psi^{-1}(0) = {\varphi_1}^{-1}(0). \tag{21}$$

Note that the solution ψ of the above equation is a level set function, but is not a distance map. Now, the advancing crack front location at any time Δt later is given by the level curve $\psi^{-1}(\Delta t)$. The advantage of this technique over a standard level set method approach is that an arbitrarily large time step Δt can be taken without introducing instability and the method is second-order accurate. This is ideal for a problem such as crack propagation where computation of the speed is very expensive and accuracy of the distance map φ_1 is critical to obtaining good approximations for the speed.

(7) The FMM is again used to solve

$$\|\boldsymbol{\nabla}\varphi_1\| = 1, {\varphi_1}^{-1}(0) = \psi^{-1}(0) \tag{22}$$

to reconstruct the distance funtion φ_1.

(8) if $t < t_{max}$, then increment t ($t \leftarrow t + 1$) and goto step 2.

6 Governing equations

6.1 Strong Form

Consider a body $\Omega \subset \mathbb{R}^3$, with boundary Γ (Fig. 8). The boundary Γ consists of the sets Γ_u, Γ_t, and Γ_c^i, such that $\Gamma = \Gamma_u \cup \Gamma_t \cup_{i=1}^m \Gamma_c^i$. All the internal surfaces Γ_c^i are assumed to be traction-free.

The field equations of elastostatics are:

$$\boldsymbol{\nabla} \cdot \boldsymbol{\sigma} + \mathbf{b} = 0 \quad \text{in} \quad \Omega, \tag{23a}$$

$$\boldsymbol{\sigma} = \mathbf{C} : \boldsymbol{\varepsilon}, \tag{23b}$$

$$\boldsymbol{\varepsilon} = \boldsymbol{\nabla}_s \mathbf{u}, \tag{23c}$$

where $\boldsymbol{\nabla}_s$ is the symmetric gradient operator, $\mathbf{u}$ is the displacement vector, $\boldsymbol{\varepsilon}$ is the small strain tensor, $\boldsymbol{\sigma}$ is the Cauchy stress tensor, $\mathbf{b}$ is the body force vector per unit volume, and $\mathbf{C}$ is the tensor of elastic moduli for a homogeneous isotropic material.

The essential and natural boundary conditions are:

$$\mathbf{u} = \bar{\mathbf{u}} \quad \text{on} \quad \Gamma_u, \tag{24a}$$

$$\boldsymbol{\sigma} \cdot \mathbf{n} = \bar{\mathbf{t}} \quad \text{on} \quad \Gamma_t, \tag{24b}$$

$$\boldsymbol{\sigma} \cdot \mathbf{n} = 0 \quad \text{on} \quad \Gamma_c^i, \quad (i = 1, 2, \ldots, m), \tag{24c}$$

where $\mathbf{n}$ is the unit outward normal to Ω, $\bar{\mathbf{u}}$ and $\bar{\mathbf{t}}$ are prescribed displacements and tractions, respectively, and m is the number of internal surfaces. Note that Eq. (24c) imposes the condition that the internal surfaces Γ_c^i be traction-free.

6.2 Weak Form and Discrete Equations

The weak form (principle of virtual work) for linear elastostatics is stated as: Find $\mathbf{u}^h \in \mathbf{V}^h$ such that

$$\int_{\Omega^h} \boldsymbol{\sigma}(\mathbf{u}^h) : \boldsymbol{\varepsilon}(\mathbf{v}^h)\, d\Omega = \int_{\Omega^h} \mathbf{b} \cdot \mathbf{v}^h\, d\Omega + \int_{\Gamma_t^h} \bar{\mathbf{t}} \cdot \mathbf{v}^h\, d\Gamma \quad \forall \mathbf{v}^h \in \mathbf{V}_0^h, \tag{25}$$

where $\mathbf{u}^h(\mathbf{x}) \in \mathbf{V}^h$ and $\mathbf{v}^h(\mathbf{x}) \in \mathbf{V}_0^h$ are the approximating trial and test functions used in the X-FEM. The space $\mathbf{V}^h$ is the enriched finite element space that satisfy the essential boundary conditions, and which include basis functions that are discontinuous across the crack surfaces. The space $\mathbf{V}_0^h$ is the corresponding space with homogeneous essential boundary conditions.

The trial and test functions, which are based on Eq. (12) are:

$$\mathbf{u}^h(\mathbf{x}) = \sum_{\substack{I \\ n_I \in \mathbf{N}}} \phi_I(\mathbf{x})\mathbf{u}_I + \sum_{\substack{J \\ n_J \in \mathbf{N}^c}} \phi_J(\mathbf{x})H(\mathbf{x})\mathbf{a}_J + \sum_{\substack{K \\ n_K \in \mathbf{N}^f}} \phi_K(\mathbf{x}) \left(\sum_{l=1}^{4} \psi_l(\mathbf{x})\mathbf{b}_K^l \right), \tag{26}$$

$$\mathbf{v}^h(\mathbf{x}) = \sum_{\substack{I \\ n_I \in \mathbf{N}}} \phi_I(\mathbf{x})\mathbf{v}_I + \sum_{\substack{J \\ n_J \in \mathbf{N}^c}} \phi_J(\mathbf{x})H(\mathbf{x})\mathbf{c}_J + \sum_{\substack{K \\ n_K \in \mathbf{N}^f}} \phi_K(\mathbf{x}) \left(\sum_{l=1}^{4} \psi_l(\mathbf{x})\mathbf{e}_K^l \right), \tag{27}$$

where $\phi_I(\mathbf{x})$ are the finite element shape functions, and $\psi_j(\mathbf{x})$ (j = 1–4) are the enriched functions for the crack front, which are given in Eq. (8). On substituting the trial and test functions in the weak form given in Eq. (25),

and using a standard Galerkin procedure, the discrete linear system $\mathbf{Kd} = \mathbf{f}$ is obtained. For further details, the interested reader can refer to [40].

7 Numerical Examples

We present fatigue crack propagation simulations of multiple cracks to demonstrate the versatility of the proposed technique. In all problems, numerical integration is carried out using Gauss-Legendre quadrature. In hexahedral elements associated with only the finite element shape functions, $2 \times 2 \times 2$ quadrature is used, and in elements that also have enriched degrees of freedom, $6 \times 6 \times 6$ quadrature is used. The elastic constants used in the computations are: Young's Modulus $E = 10^5$ and Poisson's ratio $\nu = 0.3$. The finite element public-domain package `gmsh` [30] is used in the finite element mesh generation.

Fatigue crack growth studies of coplanar cracks are carried out using the Paris law. The Paris exponent m is assumed to be 3 ($m = 2$–4 are typical values for metals). Unless otherwise stated, we use a mesh that consists of $24 \times 24 \times 24$ hexahedral elements for all simulations. The mesh spacing in the vicinity of the crack front is about five per cent of that near the boundary of the domain (Fig. 4).

For the examples considered in this paper, a $2 \times 2 \times 2$ hexahedral mesh with domain dimensions of $0.01 \times 0.01 \times 2a$ is constructed around the crack front to compute the stress intensity factors (a is the semi-major axis for an elliptical crack). The stress intensity factors are computed at $n = 18m$ (see Section 5.4) points on the crack front, where m is the number of initial cracks. For example, for a single penny crack, the normal velocity is evaluated at eighteen ($n = 18$) points on the crack front, whereas for two elliptical cracks, it is computed at thirty-six ($n = 36$) points on the crack front of the evolving cracks. The SIFs on the crack front are required to compute the normal velocity of the front which is used in the fast marching method to update the signed distance functions φ_1^i ($i = 1, \ldots, m$), where m is the number of cracks.

7.1 Discretization in the Fast Marching Method

For the fast marching method, we use a 1000×1000 rectilinear grid with bilinear interpolation in each grid cell. This might be considered to be prohibitively expensive, however, the efficiency of the FMM means these computations form only a tiny fraction of the overall simulation time. In return for the more refined mesh, it was shown in [39], that on using such a refined grid the SIFs were computed within 10^{-4} per cent of the values obtained using the exact

geometric description. While a less refined mesh could in principle be used, we find the marginal increase in speed to not be worth the potential decrease in accuracy.

7.2 Comparison with Using Mesh-Generation Algorithms

The algorithm presented here is one technique for propagating cracks. An alternative approach is to employ traditional finite element-based techniques coupled with an automatic mesh-generation tool. Today, three-dimensional tetrahedral mesh generation has reached a fairly sophisticated state of development. Complex meshes can typically be generated within minutes [2,4]. However, in the case of three-dimensional crack modeling, a mesh with gradual changes in the mesh size is desired, where the mesh size may vary from $O(1)$ on the external boundaries to $O(10^{-4})$ or less near the crack front in order to obtain accurate stress intensity factors [16]. In this case, adaptive refinement is required with careful control of the aspect ratios of the finite elements: bad aspect ratios can lead to poor finite element approximations and loss of accuracy. Adaptive unstructured meshing algorithms in three dimensions prove to be more challenging. The mesh generation problem for domains with rapidly evolving surfaces is still open, and few if any robust algorithms are available at this time. Such problems are of interest in crash simulation, aeroelasticity, crack propagation, and metal forging applications. For a recent approach in this direction, see [3].

The approach presented in this paper offers several advantages over automatic mesh generation. In comparison to automatic mesh generation methods, the X-FEM method offers good accuracy on comparatively course meshes. This means there are potential savings in computational cost to achieve the same level of accuracy. Also, this method provides greater flexibility for different types of discontinuous fields, making it possible to model cracks in isotropic as well as bimaterial media. Finally, the X-FEM approach can treat multiple cracks with arbitrary orientation in three dimensions without any user intervention.

It is difficult to compare the computational cost of the X-FEM method with mesh generation techniques. In the X-FEM method, the mesh generation task is simpler: the mesh must only conform to the domain, and is generated only once. By comparison, the FEM with mesh generation must regenerate the mesh each time step, including both the domain boundary and the internal discontinuities such as the crack. On the other hand, for comparable meshes, the X-FEM method will take longer each step due to the increased number of degrees of freedom from enrichment. For comparison purposes, the calculation in Fig. 1 required about 30 minutes per time step. In the final analysis, for the

single crack, the total computational cost for both methods are comparable for similar mesh densities [31].

7.3 Fatigue Growth of Coplanar Cracks

Numerical simulations of fatigue crack growth of coplanar multiple cracks are presented. In order to demonstrate the merging and evolution of multiple cracks, we consider the problem of multiple planar cracks embedded in full space under a uniform oscillating (in time) tension $\sigma^0_{33} = 1$. The coordinate axis x_3 is normal to the plane of the crack. Three examples are considered: two penny-shaped cracks, two elliptical cracks, and three penny-shaped cracks. In all examples, the numerical model consists of a finite body (bi-unit cube) with the cracks embedded inside the cube. The crack dimensions are typically a tenth or less of the specimen dimensions, and hence finite-specimen effects are minimal initially. Due to crack interactions, there are variations in the SIFs along the crack fronts. The effect of fatigue is to smooth out these variations so that after merger and growth, it evolves towards a penny-shape (if one neglects boundary effects) with a constant K_I along the crack front.

7.3.1 Two Penny-Shaped Cracks

Consider two penny-shaped cracks of radii $a = 0.05$ that are a distance $d = 0.05$ apart. Unit tractions are specified on the surfaces $x_3 = \pm 1$. Crack growth simulations are carried out for 57 steps, and the results for the evolution of the cracks are shown in Fig. 9. The location of the crack fronts before and after merger are shown in Fig. 9b, and in addition a few intermediate configurations are shown in Fig. 9c. As one can observe from Fig. 9d, the crack front shape is nearly circular after 57 steps.

In order to test the algorithm and the accuracy of the proposed technique, we also conducted crack growth simulations using an unstructured tetrahedral mesh. The tetrahedral mesh we used is shown in Fig. 10a, which consists of 19203 elements; the element size on the boundary is 0.5 and that in the vicinity of the crack front is 0.03 (Fig. 10b). The crack growth simulation results are shown in Figs. 10c and 10d. On comparing the above to the results obtained using the hexahedral mesh (Figs. 9b and 9d), we note that both simulation results are in good agreement. Hence, the results using, both, structured and unstructured meshes are consistent with each other for the evolution of the crack front.

7.3.2 Two Elliptical Cracks

In this example, two elliptical cracks of semi-major and semi-minor axes of $a = 0.08$ and $b = 0.04$, respectively, are considered. The distance between the cracks along the semi-major axis is $d = 0.04$. Unit tractions are specified on the surfaces $x_3 = \pm 1$. The nodal enrichments for the case of a single elliptical crack is shown in Fig. 5 ($a = 0.1$; $b = 0.05$). The same mesh is used in this example; however, two cracks lie on the $x_3 = 0$ plane, with only 5–6 finite elements spanning the major axis of each elliptical crack. The simulation results for the evolution of the cracks under fatigue crack growth is shown in Fig. 11. The computations are carried out for 80 steps. The evolution of the crack front is plotted in Figs. 11a–11d. The merger of the two crack and the subsequent growth of a single crack front is readily handled using the X-FEM/FMM technique. In spite of some of the computational difficulties just before the merger (see Section 5.3), the results in Fig. 9 for the growth of two penny cracks as well as the simulations presented in Fig. 11 for elliptical cracks, do indicate that the expected trends are qualitatively captured.

7.3.3 Three Penny-Shaped Cracks

In this example, we consider three penny-shaped cracks of radii $a = 0.05$ (step 1 in Fig. 12). Unit tractions are specified on the surfaces $x_3 = \pm 1$. The crack growth simulations are carried out for 20 steps, using a maximum increment that was 30 per cent of the characteristic dimension of the crack ($\Delta a_{max} = 0.0015$). The simulation results are shown in Fig. 12, with the zero level set contours indicated at some of the intermediate steps during the evolution. One can observe that the crack front assumes a near circular shape after 20 steps. The zero level set contours shown in Fig. 12 are less smooth than the simulations presented for the previous two problems. The waviness in the crack front profile is due to the choice of a larger crack growth increment than the earlier examples. A larger Δa_{max} was used so that the merger of the cracks could occur with a well-defined and single crack front with no disconnected regions of the crack ($\varphi_1 < 0$) in the interior; such implementational issues were addressed in Section 5.3.

8 Conclusions

A numerical technique for modeling fatigue crack propagation of multiple coplanar cracks was presented. In the proposed method, the Extended Finite Element Method (X-FEM) [40] was coupled to the Fast Marching Method (FMM) [32,33]. In the X-FEM, a discontinuous function and the 2-dimensional near-tip displacement fields are added to the finite element approximation to

account for the crack using the notion of partition of unity. This enables the domain to be modeled by finite elements with no explicit meshing of the crack surfaces. Hence, fatigue crack propagation can be simulated without any user-intervention or the need to remesh as the crack advances.

The level set method is a numerical technique for tracking moving interfaces [28]. The related fast marching method [32] is a computationally attractive alternative for strictly monotonically advancing fronts. In both methods, the evolving interface is represented as a level contour of a function of one higher dimension (i.e., $\varphi(\mathbf{x}) = C$). In the FMM, the motion of the interface is embedded in the solution of a static Hamilton-Jacobi equation in terms of $\varphi(\mathbf{x})$.

In a previous study [39], the methodology, algorithm, and implementation for three-dimensional crack propagation of single cracks was introduced. In this paper, the algorithms are extended for multiple coplanar cracks. The entire crack geometry, including one or more cracks, was represented by a single signed distance (level set) function φ_1. To compute the enrichment function for distinct cracks, the distance function φ_1 was split into multiple separate distance functions, one for each connected crack front. Merging of distinct cracks was handled naturally by the fast marching method with no collision detection or mesh reconstruction required. We used the Paris crack growth law to advance the crack front.

Numerical simulations of fatigue crack propagation for multiple coplanar penny-shaped and elliptical cracks were presented. The initial characteristic crack-dimensions were much smaller than the specimen dimension so as to minimize finite-specimen effects. In all simulations, the merging of cracks was easily resolved and the subsequent growth of a single crack front was observed. Crack growth of multiple cracks towards a penny-shape was seen, which is in qualitative agreement with the theory for embedded cracks in infinite media. The numerical technique and simulation results presented in this study point to the possibility of carrying out automated crack growth simulations of multiple cracks in structural components without the need to remesh or maintain the geometric description of the evolving crack. This is a promising alternative to existing finite element techniques for three-dimensional crack growth modeling.

The extension of the method presented here to out-of-plane crack growth is also a subject of further study. A first attempt at such a code has been undertaken by Moës et al [23,17]; however, the crack front tracking in this paper was done using the slower level set method rather than the FMM, requiring a coarser mesh for computing the signed distance function and consequently less accurate SIF calculations. Thus, implementing a FMM version for out-of-plane growth coupling the results of this paper with the work in [35] will be the subject of future research.

Acknowledgments

Parts of this work were completed during the summer of 2001, when N.S. was visiting the Princeton Materials Institute; the hospitality extended to him by David Srolovitz at Princeton University is appreciated.

References

[1] D. Adalsteinsson and J. A. Sethian. The fast construction of extension velocities in level set methods. *Journal of Computational Physics*, 148(1):2–22, 1999.

[2] T. J. Baker. Triangulations, mesh generation and point placement strategies. In D. A. Caughey and M. M. Hafez, editors, *Frontiers of Computational Fluid Dynamics*, pages 101–115, New York, NY, 1994. John Wiley & Sons.

[3] T. J. Baker. Mesh movement and metamorphosis. In *Proceedings of the* 10*th International Meshing Roundtable*, page Available at `http://www.imr.sandia.gov/papers/imr10/baker01.ps.gz`, Newport Beach, CA, 2001. also to appear in *Engineering with Computers (2002)*.

[4] T. J. Baker and J. C. Vassberg. Tetrahedral mesh generation and optimization. In *Proceedings of the* 6*th International Conference on Numerical Grid Generation*, pages 337–349, 1998.

[5] T. Belytschko and T. Black. Elastic crack growth in finite elements with minimal remeshing. *International Journal for Numerical Methods in Engineering*, 45(5):601–620, 1999.

[6] M. Bonnet, G. Maier, and G. Polizzotto. Symmetric Galerkin boundary element method. *Applied Mechanics Review*, 51:669–704, 1998.

[7] B. J. Carter, P. A. Wawrzynek, and A. R. Ingraffea. Automated 3-d crack growth simulation. *International Journal for Numerical Methods in Engineering*, 47:229–253, 2000.

[8] D. L. Chopp. Some improvements of the fast marching method. *SIAM Journal on Scientific Computing*, 23(1):230–244, 2001.

[9] D. N. Dai, D. A. Hills, and D. Nowell. Modelling of growth of three-dimensional cracks by a continuous distribution of dislocation loops. *Computational Mechanics*, 19:538–544, 1997.

[10] C. Daux, N. Moës, J. Dolbow, N. Sukumar, and T. Belytschko. Arbitrary cracks and holes with the extended finite element method. *International Journal for Numerical Methods in Engineering*, 48(12):1741–1760, 2000.

[11] G. Dhondt. Automatic 3-D mode I crack propagation calculations with finite elements. *International Journal for Numerical Methods in Engineering*, 41(4):739–757, 1998.

[12] C. A. Duarte, I. Babuška, and J. T. Oden. Generalized finite element methods for three dimensional structural mechanics problems. *Computers and Structures*, 77:215–232, 2000.

[13] C. A. Duarte, O. N. Hamzeh, T. J. Liszka, and W. W Tworzydlo. The element partition method for the simulation of three-dimensional dynamic crack propagation. *Computer Methods in Applied Mechanics and Engineering*, 190(15–17):2227–2262, 2001.

[14] M. Fleming, Y. A. Chu, B. Moran, and T. Belytschko. Enriched element-free Galerkin methods for crack tip fields. *International Journal for Numerical Methods in Engineering*, 40:1483–1504, 1997.

[15] W. H. Gerstle, A. R. Ingraffea, and R. Perucchio. Three-dimensional fatigue crack propagation analysis using the boundary element method. *International Journal of Fatigue*, 10(3):187–192, 1988.

[16] M. Gosz, J. Dolbow, and B. Moran. Domain integral formulation for stress intensity factor computation along curved three-dimensional interface cracks. *International Journal of Solids and Structures*, 35:1763–1783, 1998.

[17] A. Gravouil, N. Moës, and T. Belytschko. Non-planar 3D crack growth by the extended finite element and the level sets – Part II: Level set update. *International Journal for Numerical Methods in Engineering*, 53(11):2569–2586, 2002.

[18] D. A. Hills, P. A. Kelly, D. N. Dai, and A. M. Korsunsky. *Solution of Crack Problems: The Distributed Dislocation Technique*. Kluwer Academic Publishers, Dordrecht, The Netherlands, 1996.

[19] H. Ji, D. Chopp, and J. E. Dolbow. A hybrid extended finite element/level set method for modeling phase transformations. *International Journal for Numerical Methods in Engineering*, 54(8):1209–1233, 2002.

[20] J. M. Melenk and I. Babuška. The partition of unity finite element method: Basic theory and applications. *Computer Methods in Applied Mechanics and Engineering*, 139:289–314, 1996.

[21] Y. Mi and M. H. Aliabadi. Three-dimensional crack growth simulations using BEM. *Computers and Structures*, 52(5):871–878, 1994.

[22] N. Moës, J. Dolbow, and T. Belytschko. A finite element method for crack growth without remeshing. *International Journal for Numerical Methods in Engineering*, 46(1):131–150, 1999.

[23] N. Moës, A. Gravouil, and T. Belytschko. Non-planar 3D crack growth by the extended finite element and level sets. Part I: Mechanical model. *International Journal for Numerical Methods in Engineering*, 53(11):2549–2568, 2002.

[24] B. Moran and C. F. Shih. Crack tip and associated domain integrals from momentum and energy balance. *Engineering Fracture Mechanics*, 27(6):615–641, 1987.

[25] G. P. Nikishkov and S. N. Atluri. Calculation of fracture mechanics parameters for an arbitrary three-dimensional crack by the 'equivalent domain integral method'. *International Journal for Numerical Methods in Engineering*, 24:1801–1821, 1987.

[26] T. Nishioka and S. N. Atluri. Analytical solution for embedded cracks, and finite element alternating method for elliptical surface cracks, subjected to arbitrary loading. *Engineering Fracture Mechanics*, 17:247–268, 1983.

[27] J. T. Oden, C. A. Duarte, and O. C. Zienkiewicz. A new cloud-based *hp* finite element method. *Computer Methods in Applied Mechanics and Engineering*, 153(1–2):117–126, 1998.

[28] S. Osher and J. A. Sethian. Fronts propagating with curvature-dependent speed: Algorithms based on Hamilton-Jacobi formulations. *Journal of Computational Physics*, 79(1):12–49, November 1988.

[29] P. C. Paris, M. P. Gomez, and W. E. Anderson. A rationale analytic theory of fatigue. *The Trend in Engineering*, 13(1):9–14, 1961.

[30] J.-F. Remacle and C. Geuzaine. *Gmsh finite element grid generator*. Available at `http://scorec.rpi.edu/~remacle/Gmsh_Eng.html`, 1998.

[31] W. T. Riddell, A. R. Ingraffea, and P. A. Wawrzynek. Experimental observations and numerical predictions of three-dimensional fatigue crack propagation. *Engineering Fracture Mechanics*, 58(4):293–310, 1997.

[32] J. A. Sethian. A marching level set method for monotonically advancing fronts. *Proceedings of the National Academy of Sciences*, 93(4):1591–1595, 1996.

[33] J. A. Sethian. Fast marching methods. *SIAM Review*, 41(2):199–235, 1999.

[34] J. A. Sethian. *Level Set Methods & Fast Marching Methods: Evolving Interfaces in Computational Geometry, Fluid Mechanics, Computer Vision, and Materials Science*. Cambridge University Press, Cambridge, UK, 1999.

[35] M. Stolarska, D. L. Chopp, N. Moës, and T. Belytschko. Modeling crack growth by level sets and the extended finite element method. *International Journal for Numerical Methods in Engineering*, 51(8):943–960, 2001.

[36] T. Strouboulis, I. Babuška, and K. Copps. The design and analysis of the generalized finite element method. *Computer Methods in Applied Mechanics and Engineering*, 181(1–3):43–69, 2000.

[37] T. Strouboulis, K. Copps, and I. Babuška. The generalized finite element method. *Computer Methods in Applied Mechanics and Engineering*, 190(32–33):4081–4193, 2001.

[38] N. Sukumar, D. L. Chopp, N. Moës, and T. Belytschko. Modeling holes and inclusions by level sets in the extended finite element method. *Computer Methods in Applied Mechanics and Engineering*, 190(46–47):6183–6200, 2001.

[39] N. Sukumar, D. L. Chopp, and B. Moran. Extended finite element method and fast marching method for three dimensional fatigue crack propagation. *Engineering Fracture Mechanics*, 70(1):29–48, 2003.

[40] N. Sukumar, N. Moës, B. Moran, and T. Belytschko. Extended finite element method for three-dimensional crack modeling. *International Journal for Numerical Methods in Engineering*, 48(11):1549–1570, 2000.

[41] K. Vijayakumar and S. N. Atluri. An embedded elliptical flaw in an infinite solid, subject to arbitrary crack-face tractions. *Journal of Applied Mechanics*, 48:88–96, 1981.

[42] G. Xu and M. Ortiz. A variational boundary integral equation method for the analysis of 3d cracks of arbitrary geometry modelled as continuous distribution of dislocation loops. *International Journal for Numerical Methods in Engineering*, 31:3675–3701, 1993.

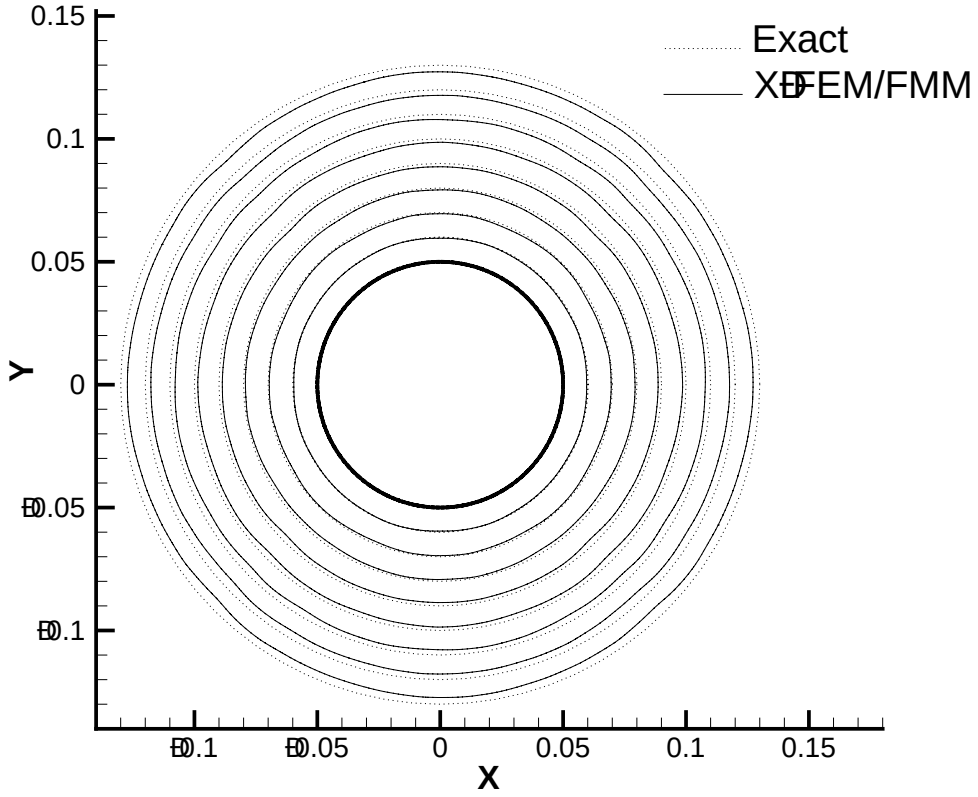

Fig. 1. Comparison of penny crack growth to the exact solution.

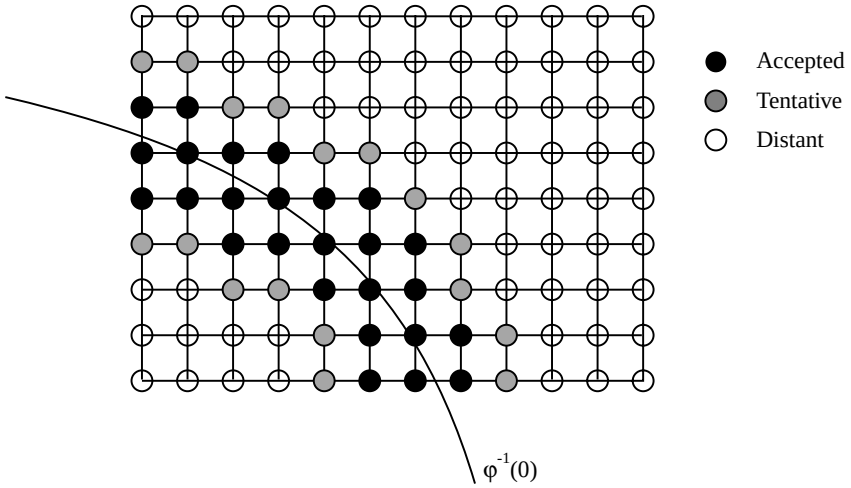

(a)

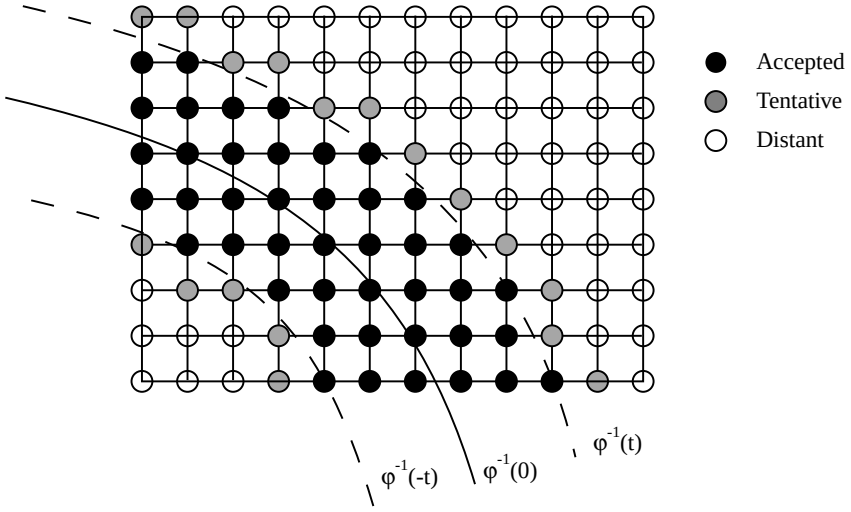

(b)

Fig. 2. Nodal sets used in the fast marching method. (a) Initial step $t = 0$; and (b) Intermediate step $t > 0$.

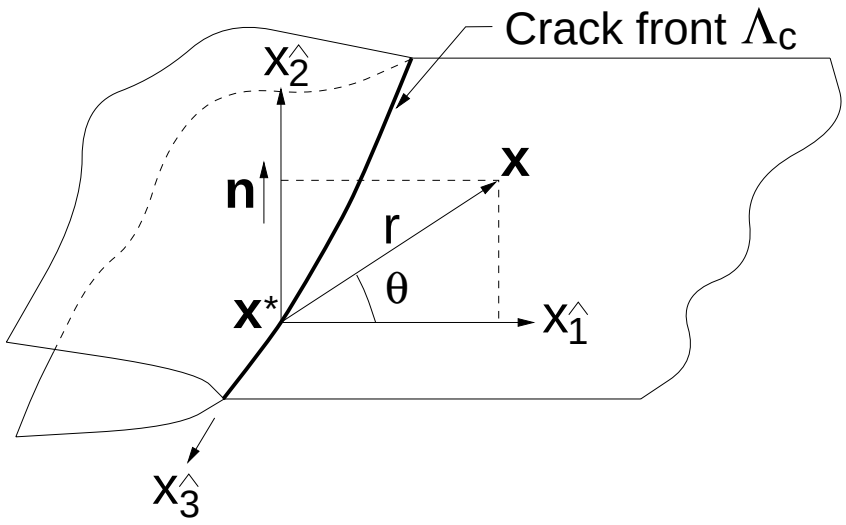

Fig. 3. Coordinate configuration for crack front enrichment functions.

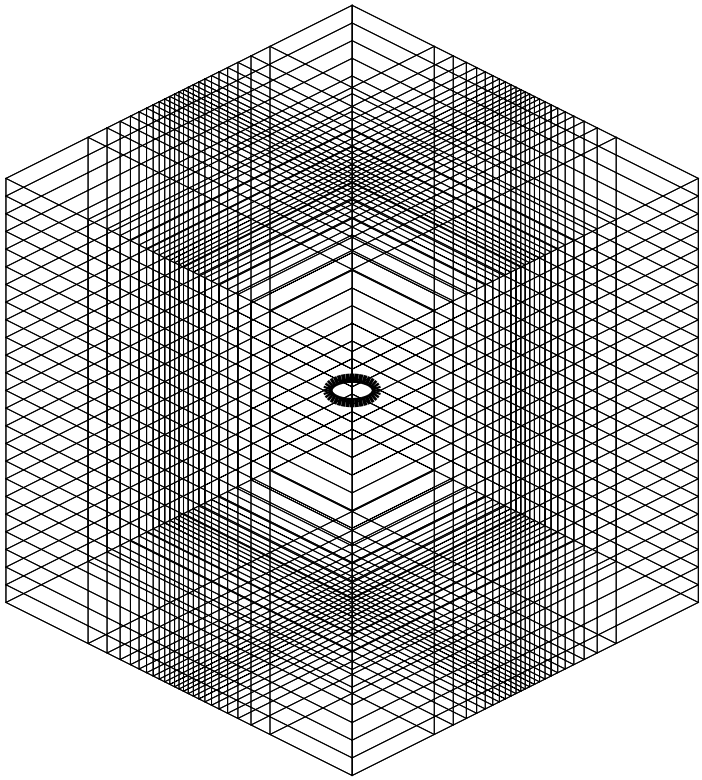

Fig. 4. Hexahedral mesh (surface) for the crack growth problems.

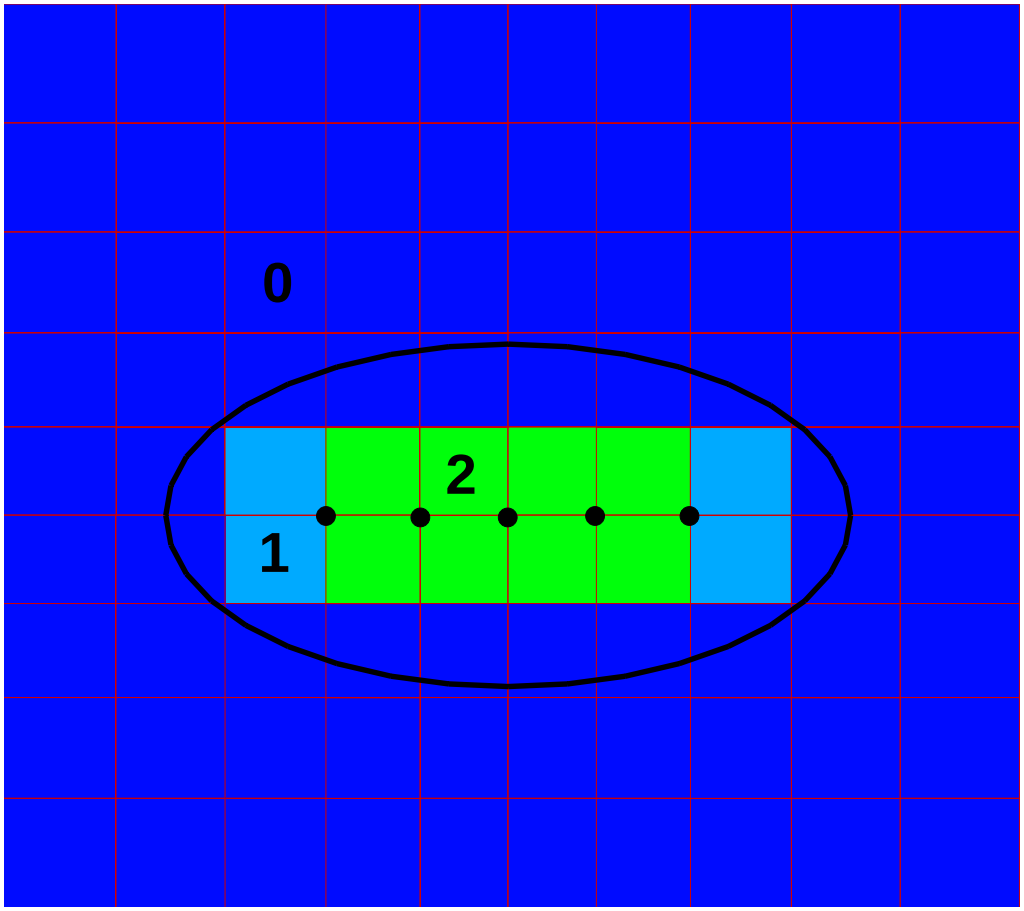

(a)

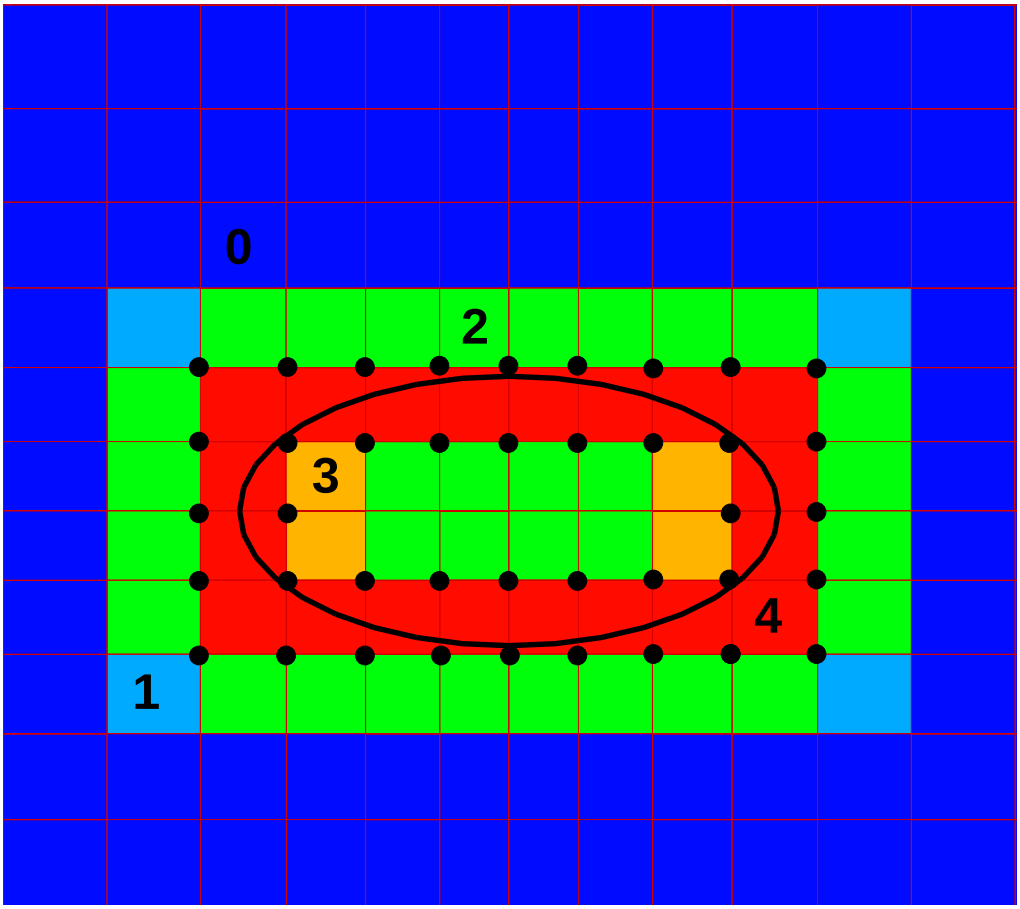

(b)

Fig. 5. Enriched nodes for an elliptical crack. The enriched nodes are indicated by filled circles and the labels denote the number of nodes enriched in each 4-noded surface element. (a) Heaviside function; and (b) Crack-front enrichment function.

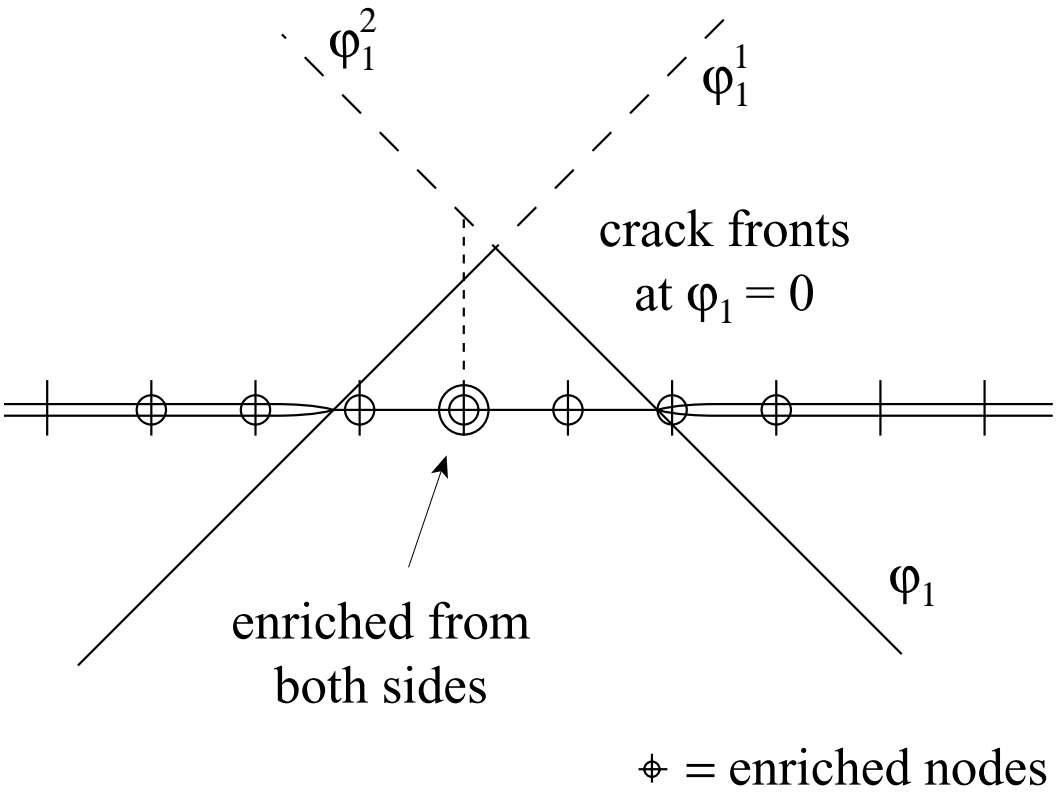

Fig. 6. Example of multiply-enriched node. Solid line is for single distance function, dashed line is for separate distance functions.

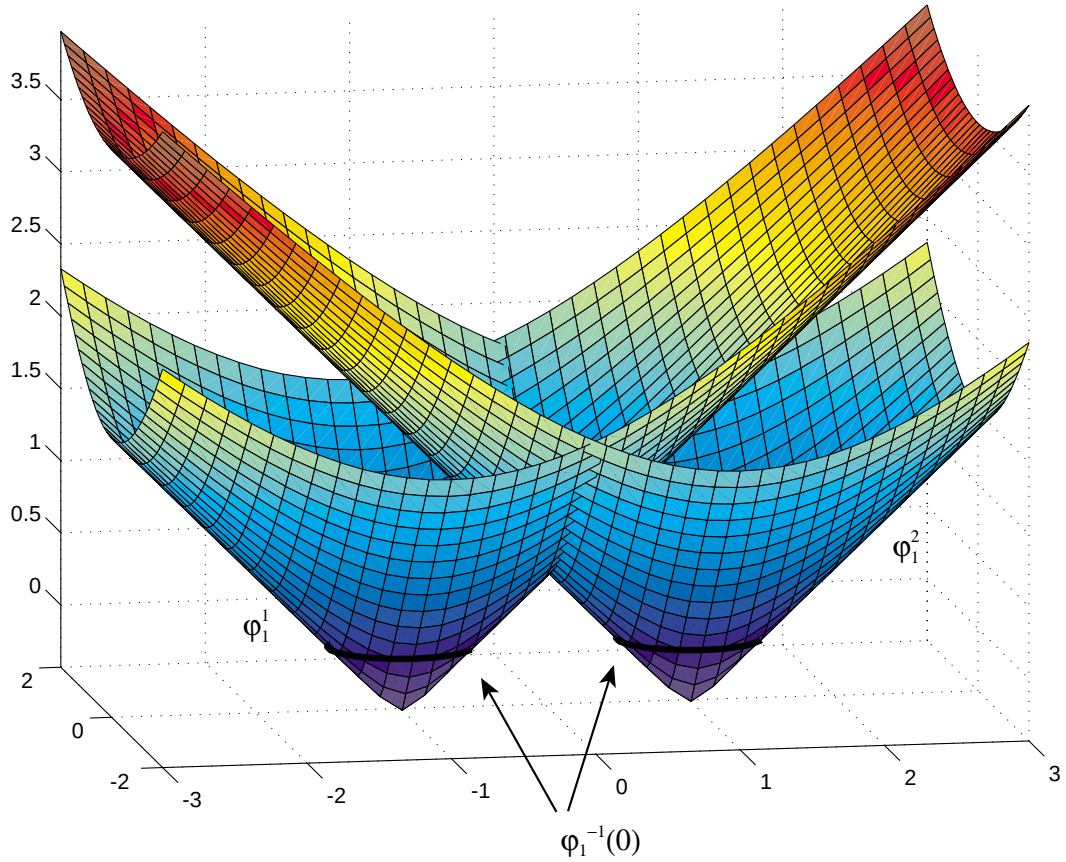

Fig. 7. Level set distance functions for two coplanar cracks.

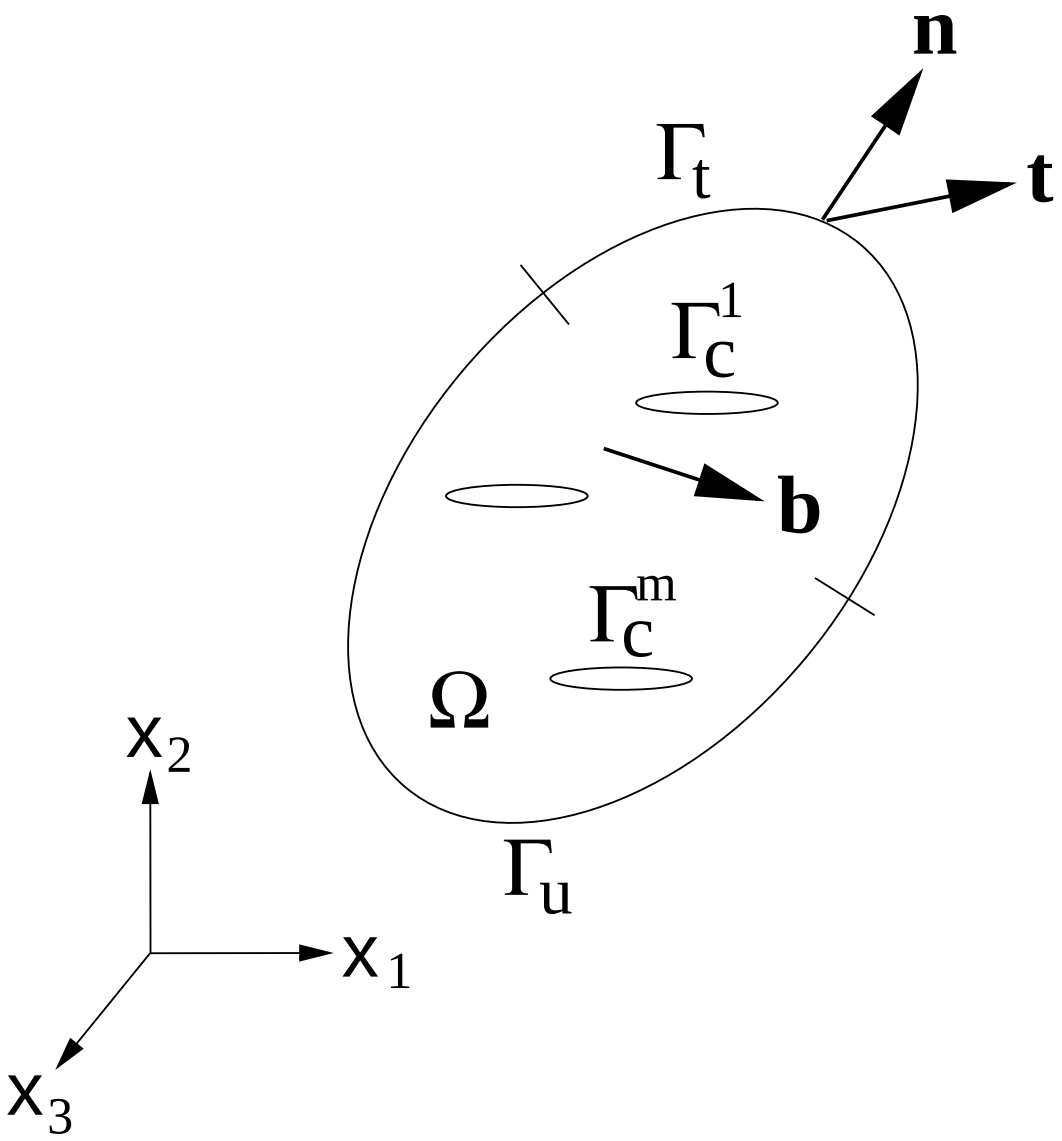

Fig. 8. Elastostatic boundary-value problem.

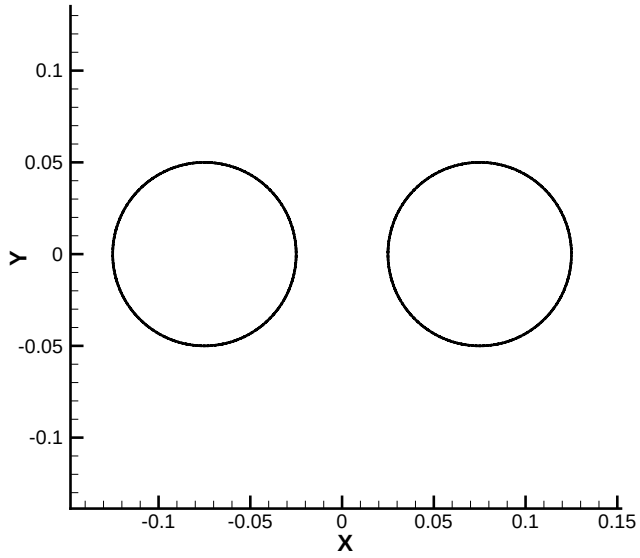
0.1
0.05
0
-0.05
-0.1
Y
-0.1
-0.05
0
0.05
0.1
0.15
X

(a)

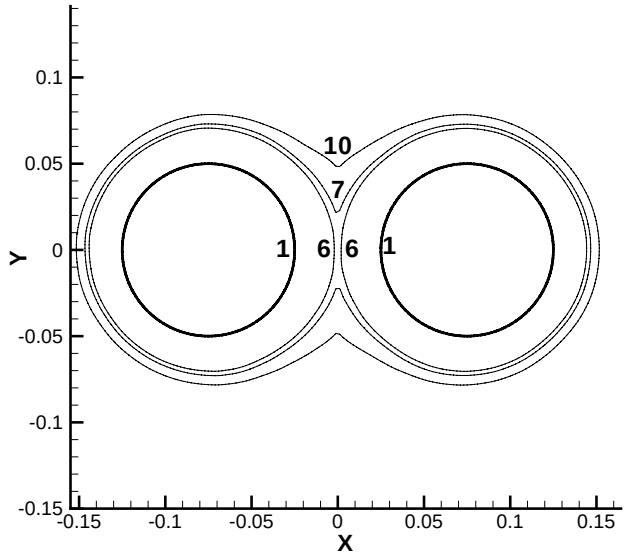
0.1
0.05
0
-0.05
-0.1
-0.15
Y
10
7
1
6
6
1
-0.15
-0.1
-0.05
0
0.05
0.1
0.15
X

(b)

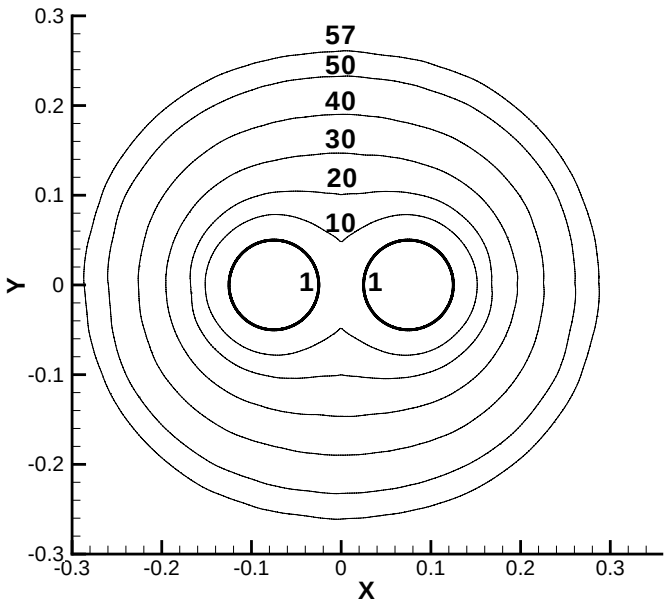

(c)

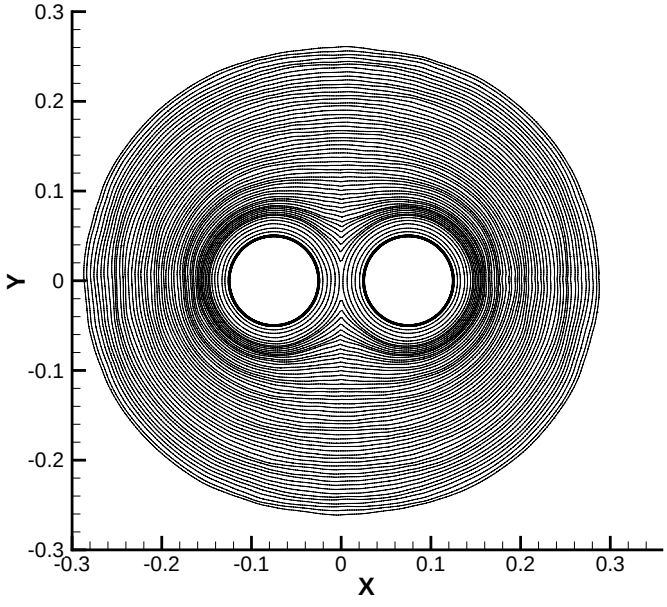

(d)

Fig. 9. Fatigue crack growth simulation of two penny-shaped cracks. The step number is indicated in the plots. (a) Initial cracks; (b) Before and after merging. (c) Intermediate configurations; and (d) Entire evolution.

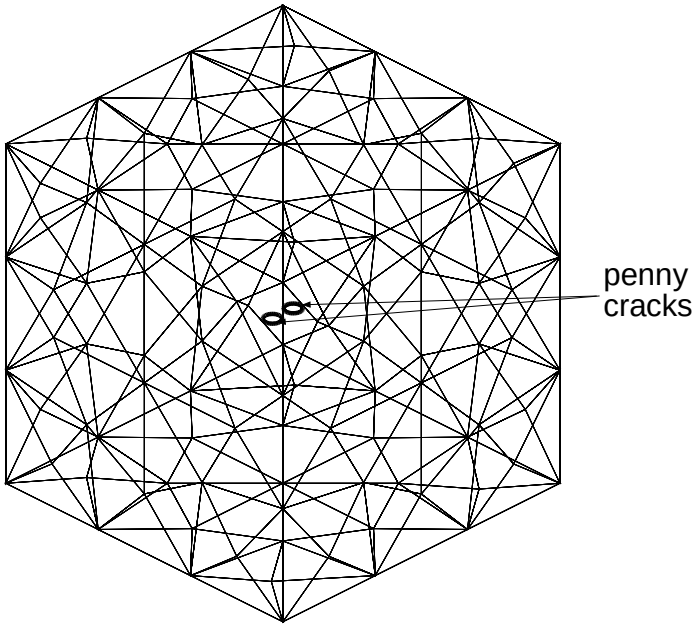

(a)

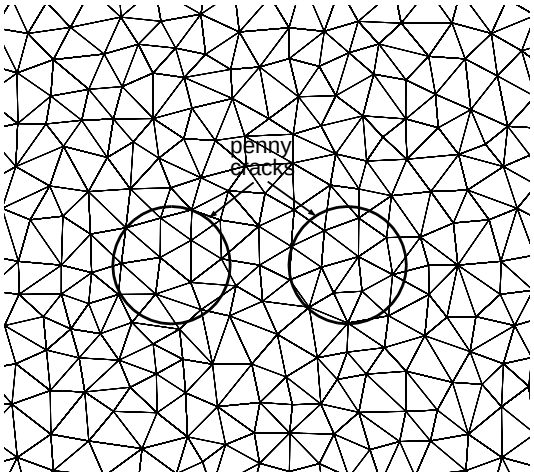

(b)

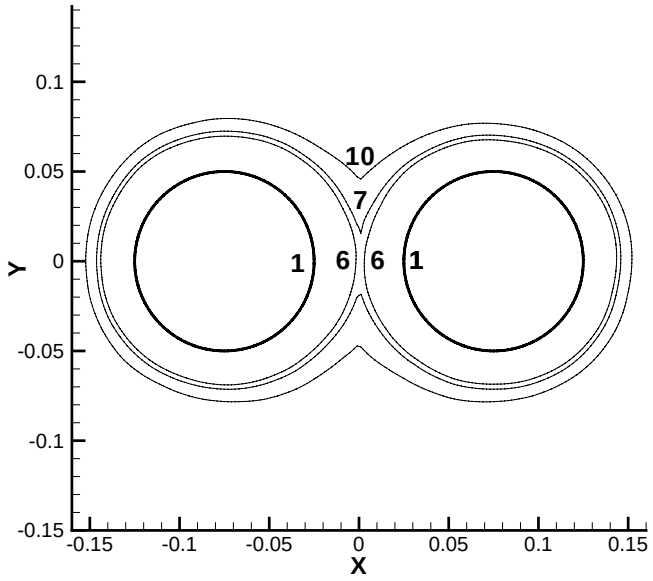

(c)

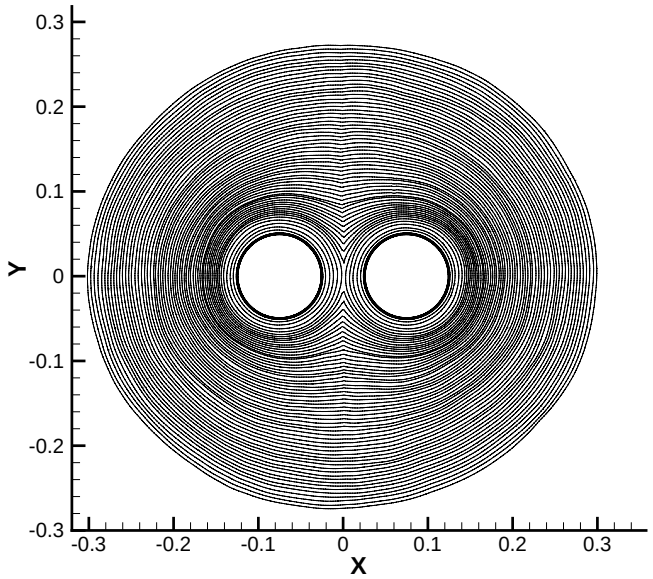

(d)

Fig. 10. Fatigue crack growth simulation of two embedded penny-shaped cracks using an unstructured mesh. (a) Boundary mesh and cracks; (b) Surface elements in the vicinity of the cracks; (c) Before and after merger (step numbers are indicated); and (d) Crack evolution (59 steps).

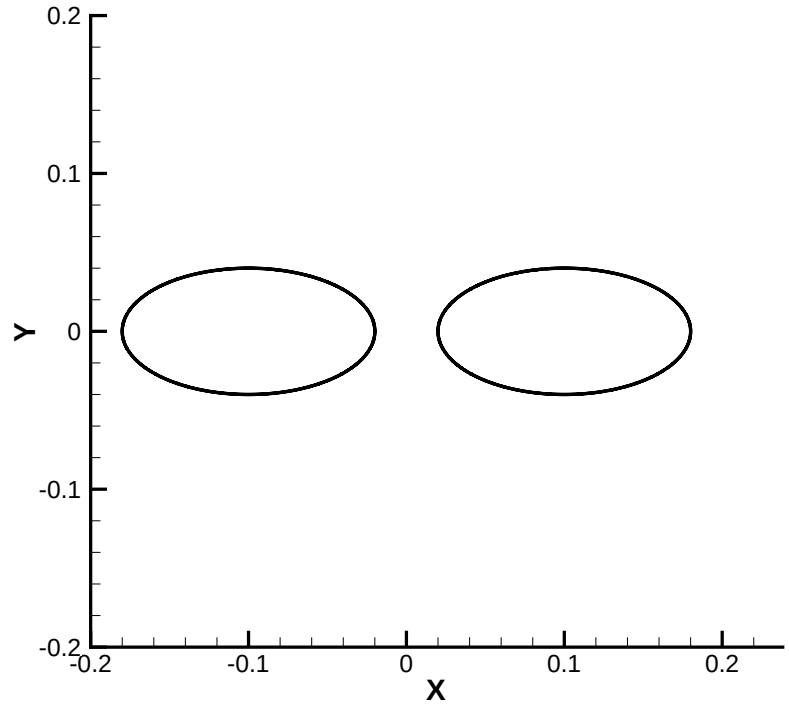

(a)

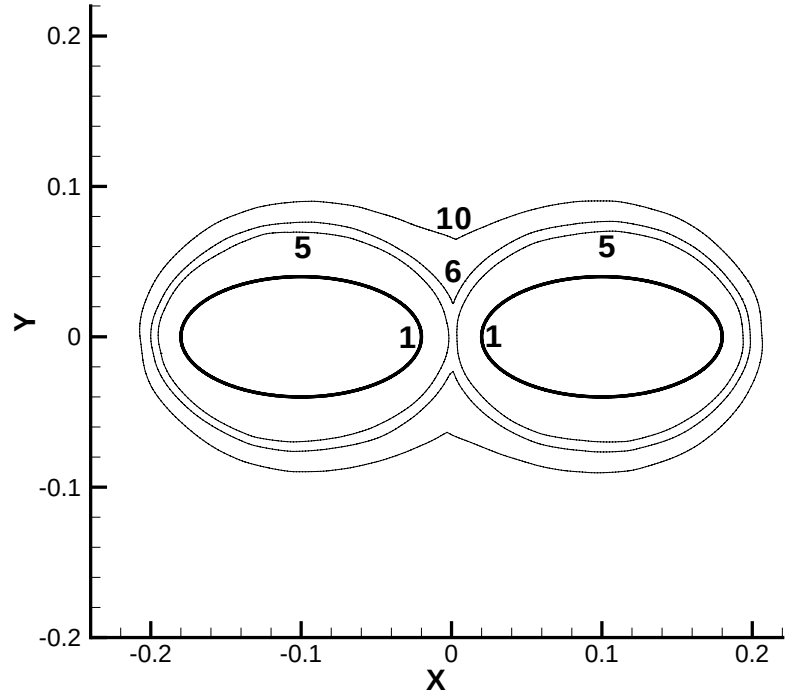

(b)

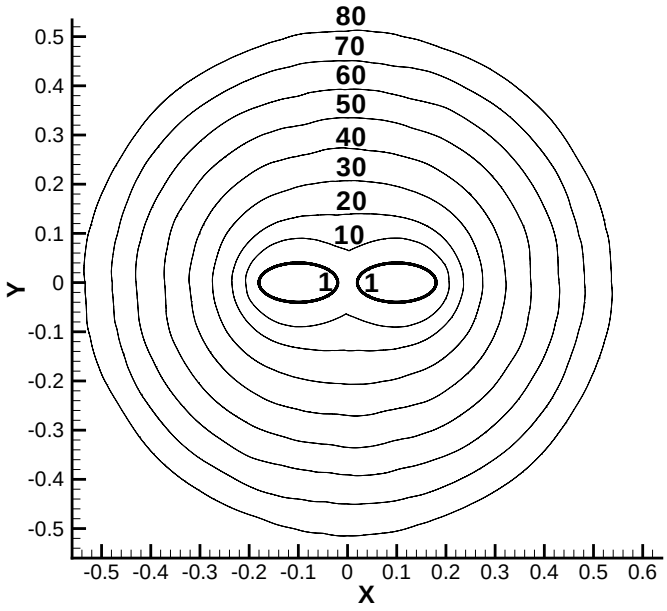

(c)

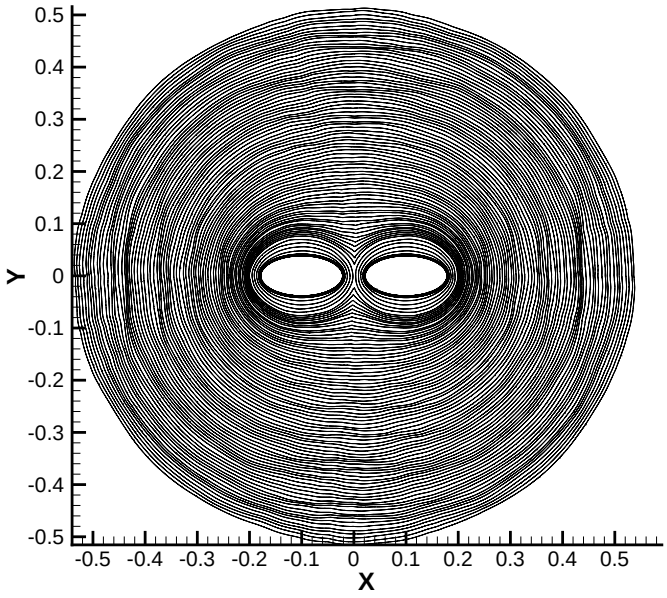

(d)

Fig. 11. Fatigue crack growth simulation of two embedded elliptical cracks. The step number is indicated in the plots. (a) Initial cracks; (b) Before and after merging. (c) Intermediate configurations; and (d) Entire evolution.

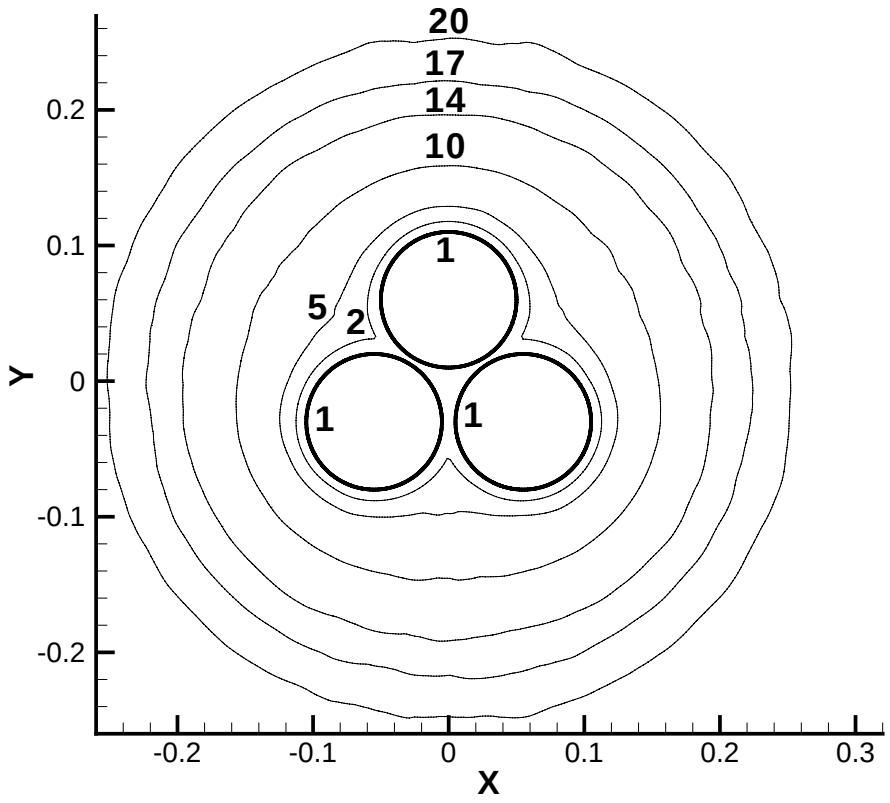

Fig. 12. Fatigue crack growth simulation of three penny-shaped cracks. The step number is indicated in the plot.